2012

Dynamics and Collective State of Ordered Magnetic Nanoparticles in Mesoporous Systems

Jose M. Vargas
University if New Orleans, jmvargas@uno.edu

Abhishek Srivastava
University of New Orleans, abhi.alld@gmail.com

Ezra Garza
University of New Orleans, epgarza@my.uno.edu

Amin Yourdkhani
University of New Orleans, ayourdkh@uno.edu

Gabriel Caruntu
University of New Orleans, gcaruntu@uno.edu

See next page for additional authors

Recommended Citation
J. Appl. Phys.112, 094309 (2012);

AIP | Journal of Applied Physics

Dynamics and collective state of ordered magnetic nanoparticles in mesoporous systems

José M. Vargas, Abhishek Srivastava, Ezra Garza, Amin Yourdkhani, Gabriel Caruntu et al.

Citation: J. Appl. Phys. **112**, 094309 (2012); doi: 10.1063/1.4764018
View online: http://dx.doi.org/10.1063/1.4764018
View Table of Contents: http://jap.aip.org/resource/1/JAPIAU/v112/i9
Published by the American Institute of Physics.

Dynamics and collective state of ordered magnetic nanoparticles in mesoporous systems

José M. Vargas,[1] Abhishek Srivastava,[1,2] Ezra Garza,[1,2] Amin Yourdkhani,[1,3] Gabriel Caruntu,[1,3] and Leonard Spinu[1,2,a)]
[1]*Advanced Materials Research Institute, University of New Orleans, New Orleans, Louisiana 70148, USA*
[2]*Department of Physics, University of New Orleans, New Orleans, Louisiana 70148, USA*
[3]*Department of Chemistry, University of New Orleans, New Orleans, Louisiana 70148, USA*

(Received 20 June 2012; accepted 9 October 2012; published online 5 November 2012)

In this paper we present a study of superparamagnetic and superspin glass states of magnetic nanoparticles confined in mesoporous templates. Characterization utilizes dynamic magnetization techniques, *ac* susceptibility, and ferromagnetic resonance, in addition to *dc* magnetization curves. In order to differentiate between the intrinsic and collective properties, we considered three magnetic nanoparticles systems with comparable size, shape, and crystallinity but with different intrinsic magnetocrystalline anisotropy. Further, confinement effects were studied by considering three different geometries of nanoparticles. The effect of the geometrical confinement and intrinsic anisotropy of the nanoparticles are discussed based on known theoretical predictions. © *2012 American Institute of Physics*. [http://dx.doi.org/10.1063/1.4764018]

I. INTRODUCTION

Collective phenomena in nanostructured magnetic materials have attracted considerable attention in the last few years in both fundamental research and technological applications.[1–4] Mainly, due to the requirements of miniaturization needed in magnetic recording media, antennas, and transducers, new magnetic features emerge and these phenomena will dominate the magnetic properties of the whole system, such as isotropic or anisotropic interactions, strong interparticle coupling, and geometrical or structural shape anisotropy induced by the host or substrates.[5,6] Therefore, if the thermal effects are significant, the magnetic nanoparticles (NPs) that build up the whole system cannot be modelled as a collection of isolated single magnetic domains, following the ideal Stoner-Wohlfarth or Néel-Brown model.[7,8] In the presence of magnetic interactions, the assembly of magnetic nanoparticles is a complicated many body problem governed by an energy landscape which is far more complex than the double-well potential corresponding to isolated magnetic monodomain particles.[9] Thus, the macroscopic properties cannot be predicted by models based only in individual particles, and a more complex modelling will be required taking into account multiple particle interactions and structural and geometrical arrangement.[10,11] The thermal magnetic relaxation process has been studied exhaustively since the works of Dormann-Fiorani[12,13] and Mørup *et al.*[14] in powder, flocculated, and isolated nanoparticles in a polymer matrix with random orientation. In all cases, the interaction effects and collective phenomena were discussed based on phenomenological models with corrections of the Arrhenius law or the Stoner-Wohlfarth model. Parker and co-workers[15] studied the low-temperature superspin-glass behavior of a concentrated frozen ferrofluid made of γ–Fe_2O_3 nanoparticles, and they found that the scaling laws normally applied to atomic spin glasses are also valid for superspin-glass samples, with good agreement between the scaling parameters for the *ac* and *dc* relaxation curves. Also, the superparamagnetism (SPM) phenomena of individual monodomain magnetic NPs can be affected by the geometrical and texturization properties of the host. For example, when magnetic particles are embedded in a ferromagnetic or antiferromagnetic matrix, stabilization is induced by the magnetic interaction between the particles and the host, which can shift the SPM limit to higher temperatures.[16,17] Regarding collective states, Butera *et al.*[18] studied a multilayer system by alternating layers of Py ($Fe_{20}Ni_{80}$) film and Fe_3O_4 NPs, following the sequence $(Py/NPs/Py)_N$. In this case, through *dc*-magnetization and ferromagnetic resonance experiments, a magnetic signal related to the collective state can be resolved. In the most basic form, isotropic collective effects in random oriented NP systems can also be expected due to dipolar interactions in powder and NPs embedded into polymer hosts. More recently, with the aim to grow multifunctional nanostructured systems, magnetic particles infiltrated into nanotubes and mesoporous hosts showed another striking source of anisotropy induced by the geometry and structure of the pores and nanotubes.[19–21] This cooperative phenomena between the columns of magnetic NPs supported within the nanotubes or porous host open a new degree of freedom to tune the magnetic properties of the whole system. For example, Olivetti *et al.*[19] studied iron-oxide NPs injected in porous anodic alumina (pore size of 20 nm and 100 nm), where the arrangement of particles in regular nanostructures of this type leads to the emergence of new properties, governed by the simultaneous presence of three relevant scales: particle size, pore diameter, and the scale of the geometrical arrangement of the template pores. Tolbert *et al.*[20] studied cobalt NPs infiltrated in hexagonal mesoporous silica, where the filling fraction effect on the magnetic properties were discussed in detail. In particular, they showed that at the nanoscale, confinement of

a)Electronic mail: LSpinu@uno.edu.

single-domain magnetic NPs in the one-dimensional pores of hexagonal mesoporous silica results in constructive magnetic interactions, and a "more coercive material is formed due to anisotropic ferromagnetic interparticle coupling within the chains of nanocrystals." Similar fabrication procedures were conducted by Jung *et al.*[21] using FePt NPs embedded in the nanochannels of an anodic alumina template, where after annealing at 700 °C, the ordered fct FePt polycrystalline nanostructure had high magnetic anisotropy and thus large coercivity up to 1.1 T at room temperature.

While studying the properties of confined magnetic nanoparticles, one of the most relevant factors is the relationship between the intrinsic anisotropy of the NPs and external anisotropy induced by the shape/geometrical arrangement of the template pores. Thus, it is conceivable that the collective behavior of the confined NPs can be tuned by a control of the intrinsic properties of NPs and their spatial arrangement. In the previous reports this connection between intrinsic and assembly magnetic properties was studied mainly by using static measurement techniques as field and temperature dependent magnetization curves. In this paper we present a study of superparamagnetic and superspin glass (SSG) states of magnetic nanoparticles confined in mesoporous templates using dynamic magnetization techniques as *ac* susceptibility and ferromagnetic resonance (FMR) in addition to *dc* magnetization curves. In order to differentiate between the intrinsic and collective properties in our study, we considered three magnetic nanoparticles systems with comparable size, shape, and crystallinity but with different intrinsic magnetocrystalline anisotropies. In addition, the confinement effects were studied by considering three different geometries of nanoparticles. Specifically, we considered Fe_3O_4, $MnFe_2O_4$, and $CoFe_2O_4$ ferrite single magnetic domain NPs with size near to 10 nm, infiltrated into AAO templates with 297 nm porous size and thickness of 50 μm, and infiltrated in an nonmagnetic AAO-BTO nanotubes with 197 nm internal porous size and same length. The effect of the geometrical confinement and intrinsic anisotropy of the NPs are discussed based on the known theoretical predictions.

II. EXPERIMENTAL

The inverse spinel ferrite NPs were synthesized using a modified high temperature thermal decomposition method published elsewhere.[22] In a typical synthesis, 1 mmol of $Fe(ac)_2$ and 0.5 mmol transition metal acetate $M(ac)_2$ (M = Mn, Fe, Co) and 6 mmols of oleic acid were added to 15 ml benzyl ether in a three-neck round bottom flask and kept under vigorous stirring. To promote the dissolution of the acetate salts and eliminate the hydrating water molecules the initial solution was heated rapidly to 150 °C and maintained at this temperature for 15 min. The temperature was subsequently increased to 275 °C. After 30 min, the reaction was stopped by removing the heat source and allowing the solution to cool down naturally to room temperature. The resulting powders were recovered from the solution by magnetic separation and then washed several times with ethanol and acetone, separated again, and extracted in hexane. For the complete removal of the excess benzyl ether, this purification protocol was repeated three times. Oleic acid-capped magnetic nanocrystals were isolated and then dispersed in various non-polar solvents (chloroform, hexane, etc.) yielding brown clear colloids which are stable against aggregation for months at room temperature. Commercial porous alumina membranes (Whatman Anodisc) with thickness of (50 ± 1) μm and mean pore-size of (297 ± 50) nm were used in this study. The membrane porosity is 41%, according to estimations made on the basis of the membrane imaging. For simplicity the anodic aluminum oxide template are abbreviated AAO. Nanotubes of barium titanate ($BaTiO_3$) were grown inside of AAO template from aqueous solutions using a simple, inexpensive, reproducible, and environmentally friendly procedure. The deposition solution is prepared by dissolving ammonium hexafluorotitanate and barium nitrate in a boric acid solution at a *p*H of 2.5. The blend is kept at the temperature of 40 °C for 12 h. After annealing at 750 °C in air, the resulting nanotubes are polycrystalline cubic $BaTiO_3$. The typical lengths of $BaTiO_3$ nanotubes are 50 μm, with an average internal diameter of approximately 197 nm, which is defined by the pore diameter and thickness of the AAO template. Hence, the average $BaTiO_3$ wall-thickness value is near 50 nm (see structural results below). In this case, the $BaTiO_3$ was labeled as BTO. Three batches of samples were prepared by the infiltration method, using the Fe_3O_4, $MnFe_2O_4$, and $CoFe_2O_4$ colloidal NPs samples. The first batch of samples corresponds to the powder NPs of each ferrite composition, respectively. For their preparation, a polar solvent (ethanol) was added to the as-prepared colloidal solution of NPs in hexane (50–50 in volume), and after mixed, the samples were centrifuged at 3000 rpm for 10 min. A pellet of NPs was extracted from each respective vial and dried in normal air conditions. The batch of powder samples were labeled as PO-ferrite. The second batch of samples corresponds to the infiltrated AAO template with each ferrite NPs. Hence, the particles were impregnated into pores by mixing 3 ml of the original synthesis solution with AAO template. After 24 h, the AAO and ferrite mixture was filtered. The composite was washed with hexane while a few drops of oleic acid were added to remove any particles from the AAO surface. The sample was washed quickly with dry methanol to passivate the particle surfaces and dried in an oven (100 °C) over 24 h. Taking into account the hole mean diameter and thickness of the AAO template, the diameter-to-length aspect ratio is $\sim 1 : 200$. As reported by Tolbert *et al.*,[20] it is worth mentioning that this infiltration method leads AAO densely filled with ferrite particles. The batch of infiltrated AAO samples was labeled as AAO-Fe_3O_4, AAO-$MnFe_2O_4$, and AAO-$CoFe_2O_4$, respectively. The third batch is associated with the infiltrated nonmagnetic BTO nanotubes supported in the AAO template with each of the respective ferrite NPs. To infiltrate the nanotubes, the same procedure (mentioned above for the AAO), was conducted. In this particular structural condition, the same geometrical arrangement of holes was kept intact, with the same length and center-to-center hole distance but with different wall-thickness and internal diameter. Taking into account the mean diameter and thickness of the AAO template, the diameter-to-length aspect ratio is $\sim 1 : 300$. The batch of infiltrated BTO nanotubes, supported in the AAO template, was labeled as BTO-Fe_3O_4, BTO-$MnFe_2O_4$, and BTO-$CoFe_2O_4$,

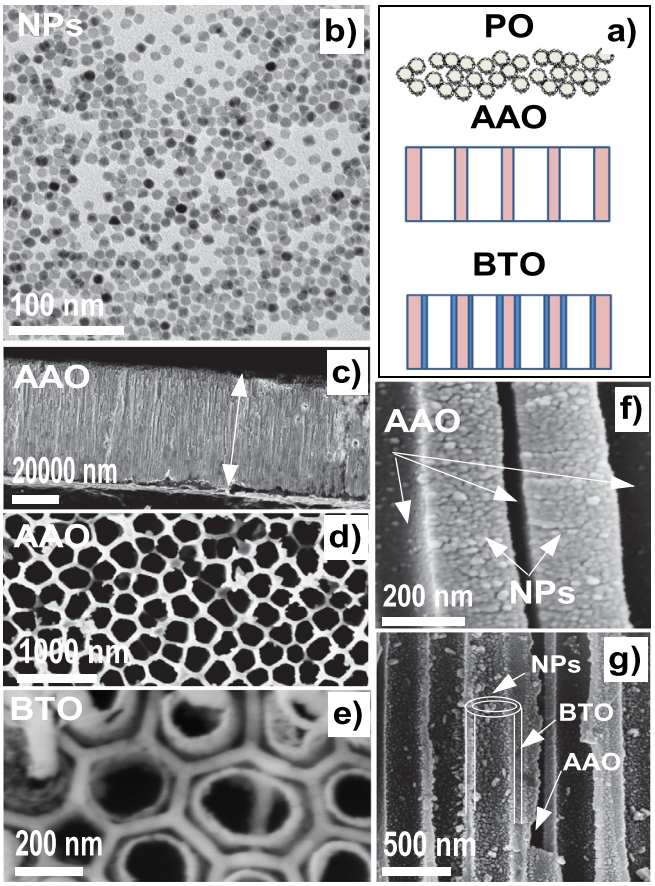

FIG. 1. (a) Schematic representation, cross-section, of the PO, AAO, and BTO samples. (b) TEM image of the $MnFe_2O_4$ NPs. (c),(d) SEM images, in cross-section and top-view, of the AAO template, respectively. (e) SEM image of the BTO nanotubes into the AAO template. (f),(g) SEM images, cross-section, of AAO and BTO infiltrated samples with $MnFe_2O_4$ NPs, respectively.

respectively. The particle size and geometrical arrangement of ferrite NPs into the AAO and BTO templates were analyzed with a JEOL JEM 2010 (200 kV) transmission electron microscope (TEM) and a Carl Zeiss 1530 VP FESEM (10 kV) scanning electron microscope (SEM). The *dc*-magnetic properties were measured using a commercial superconducting quantum interference device (SQUID) magnetometer in a temperature range of $T = 4$ K-300 K and field strength up to $H \pm 70$ kOe. The complex magnetic susceptibility $\chi = \chi' + j\chi''$ of these samples was measured as a function of temperature from 4 to 300 K for frequencies ranging from $\nu = 10$ Hz to 10 kHz in the *ac*-option of the quantum design physical property measurement system (PPMS). Ferromagnetic resonance (FMR) experiments at $\nu = 9.87$ GHz (X-band) and at room temperature were conducted using a Bruker EMX300 spectrometer.

III. RESULTS AND DISCUSSION

A. Structural characterization

Figure 1(a) shows the schematic representation of the PO, AAO, and BTO samples, respectively. Fig. 1(b) shows the TEM image of the $MnFe_2O_4$ colloidal NPs, where they evidenced a clearly high-quality crystalline order with homogeneous cubic-faceted shape. Similar results were obtained for the Fe_3O_4 and $CoFe_2O_4$ NPs.[23] The histograms of particle size distribution were built counting 200 particles for each sample (figure not shown) and fitted with a Gaussian function, $f(D) \propto \exp(-\frac{(D-\bar{D})^2}{2\sigma^2})$, where $\bar{D}$ is the center peak position and σ is the linewidth of the distribution. The mean particle sizes were determined with the values of 8.0 ± 1.5 nm ($CoFe_2O_4$ NP), 9.5 ± 0.9 nm ($MnFe_2O_4$ NP), and 6.9 ± 0.8 nm (Fe_3O_4 NP). Figures 1(c) and 1(d) correspond to the cross-section and top-view SEM images of the AAO template, respectively. The AAO pores showed circular shape with mean size of (297 ± 50) nm and interspace wall-thickness of 60 nm. Due to the limited quality in pore-size dispersion, the pores are localized randomly in a close-packing geometrical arrangement following a short-range, hexagonal-like order (Fig. 1(d)). Figures 1(f) and 1(g) show the cross-section SEM images of the infiltrated AAO template and BTO nanotubes, respectively, where it is possible to observe that the full length of the cavities was filled with ferrite nanoparticles. The BTO nanotubes are grown inside of the AAO pores, with a wall thickness value of 50 nm, which it gives an internal diameter value of 197 nm (Fig. 1(e)). For the powder ferrite NPs, the saturation magnetization, M_S, was estimated from the adjusted magnetization vs field curves at 300 K, by the Langevin formula.[23] Table I summarizes the structural and magnetic data of the ferrite

TABLE I. Structural and *dc*-magnetic properties. The errors are indicated in brackets. u is the hole internal diameter of AAO or BTO host, v is the average distance between the outside walls of the tubes, and L is the membrane thickness. SQ is the squareness of the magnetization loops.

Sample	NP size D_{TEM} (nm)	Porous template u (nm)	Porous template v (nm)	Porous template L (μm)	*Dc*-parameters H_C (Oe)	*Dc*-parameters SQ	*Dc*-parameters M_S (erg/cm^3)[a]
PO-Fe_3O_4	6.9 (0.8)	···	···	···	173	0.18	83.7 (8.3)
PO-$MnFe_2O_4$	9.5 (0.9)	···	···	···	237	0.36	78.0 (8.1)
PO-$CoFe_2O_4$	8.0 (1.5)	···	···	···	14123	0.70	68.3 (7.0)
AAO-Fe_3O_4	6.9 (0.8)	297 (50)	60 (7)	50 (1)	139	0.28	···
AAO-$MnFe_2O_4$	9.5 (0.9)	297 (50)	60 (7)	50 (1)	339	0.40	···
AAO-$CoFe_2O_4$	8.0 (1.5)	297 (50)	60 (7)	50 (1)	10136	0.70	···
BTO-Fe_3O_4	6.9 (0.8)	197 (37)	160 (20)	50 (1)	190	0.32	···
BTO-$MnFe_2O_4$	9.5 (0.9)	197 (37)	160 (20)	50 (1)	390	0.50	···
BTO-$CoFe_2O_4$	8.0 (1.5)	197 (37)	160 (20)	50 (1)	10368	0.70	···

[a]Bulk saturation magnetization values of 92 emu/g (Fe_3O_4), 80 emu/g ($MnFe_2O_4$), and 75 emu/g ($CoFe_2O_4$).[24]

NPs, AAO template, and BTO nanotubes into the AAO template.

B. Dc-magnetic characterization

For the three powder samples the *dc*-magnetization curves were measured and presented elsewhere,[23] where non-hysteresis effects were observed at room temperature (figure not shown). The magnetization loops at $T = 4$ K correspond to the case of soft (Fe_3O_4), intermediate ($MnFe_2O_4$), and hard ($CoFe_2O_4$) magnetic monodomain anisotropic materials (Fig. 2). Similar shaped magnetization loops were obtained for the infiltrated AAO and BTO ferrite samples, where the magnetic field was applied along the axis of the nanochannels. Moreover, it is important to emphasize the systematic change in the squareness, M_r/M_S, of the hysteresis loops calculated using the remanent and saturation magnetization and change in coercive fields, H_C, values that can be clearly observed for the three batches of samples: (i) In the case of Fe_3O_4 samples, the infiltrated-BTO sample shows the largest H_C. An intermediate value of H_C was measured for the PO sample, and a lower value was obtained for the infiltrated-AAO sample (Table I). (ii) For the $MnFe_2O_4$ samples, compared with the iron-oxide batch, the infiltrated-BTO sample shows the largest value of H_C. However, the infiltrated-AAO sample showed the intermediate value of H_C, and a lower value was obtained for the PO sample (Table I). (iii) In the case of $CoFe_2O_4$ samples one observes rectangular-shaped magnetization loops with very high H_C values for the PO sample. The loops for $CoFe_2O_4$ infiltrated AAO and BTO samples have almost the same H_C value lower than the PO sample (see values summarized in Table I). These *dc*-magnetization curves can be explained by taking into account the interplay between the individual and collective/cooperative magnetic contributions as the intrinsic magnetocrystalline anisotropy of the ferrite nanoparticles, the dipolar interaction between them, and the induced "needle" anisotropy due to the geometrical aspect-ratio of these samples. This is discussed in more details in the next sections.

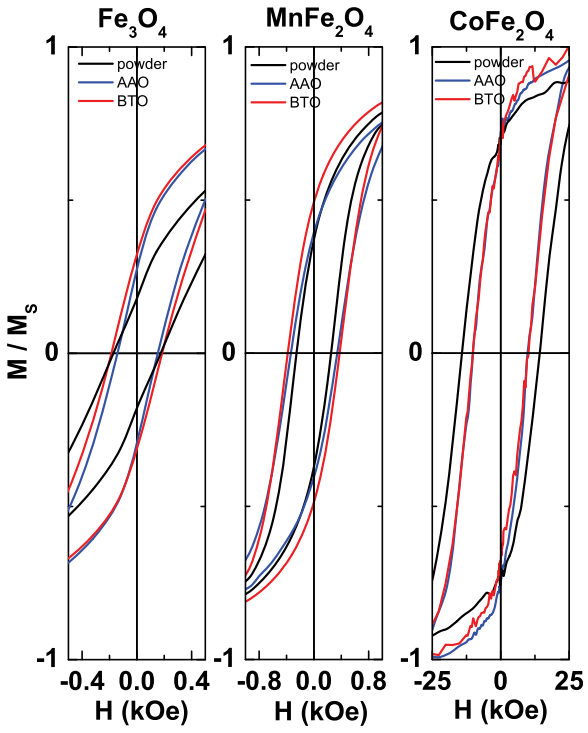

FIG. 2. Magnetization loops measured at $T = 4$ K for the three batches of ferrite samples, PO, AAO, and BTO.

C. Ferromagnetic resonance (X-band)

To confirm the cooperative and texturization phenomena on these ferrite samples, angular dependent X-band (9.87 GHz) FMR experiments were conducted at room temperature. Due to the intrinsic characteristics of the FMR technique, these experiments allowed us to get a local measurement of the effective anisotropy, resolving different anisotropy contributions with high accuracy. Figure 3 shows the FMR spectra for the AAO-Fe_3O_4 (Fig. 3 (left)), BTO-Fe_3O_4 (Fig. 3 (right)), and PO-Fe_3O_4 samples. In the case of the AAO and BTO infiltrated samples, the measurements were done with the magnetic field along the nanotubes ($H_{\|}$) and perpendicular to the nanotubes ($H_{\perp}$). The PO sample was used as the control sample, with the Fe_3O_4 nanoparticles in random orientation. Clear evidence of the cooperative phenomena and geometrical confinement influence of the AAO template and BTO nanotubes can be observed in the shape of the FMR absorption-derivative signals. These results are the clear fingerprint of textured samples and the relative strength of the intrinsic magnetic moments. To reinforce this conclusion, these results can be compared with the systematic study of the "textured sample effect" that was reported previously by Zysler *et al.*,[25] where

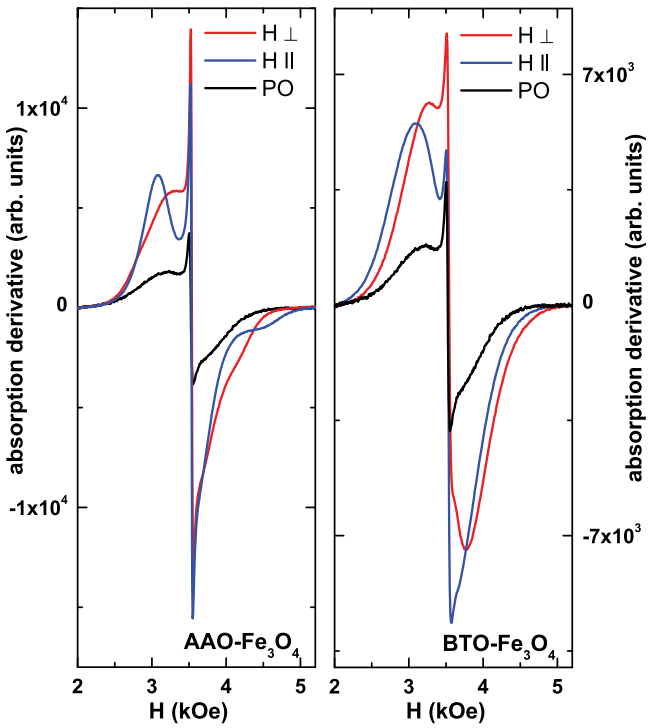

FIG. 3. X-band (9.87 GHz), FMR spectra of the Fe_3O_4 NPs infiltrated into the AAO and BTO hosts. The measurements were done with magnetic field parallel (||) and perpendicular (⊥) to the nanochannels. For reference control, the spectrum of the PO sample is added in both cases.

colloidal nanoparticles were frozen under external bias magnetic field. In this previous study, the majority of the anisotropy axes of the particles are aligned along the direction of the external magnetic field, and the assembly can be modeled as a system with a single anisotropy axis. Moreover, it was observed that the shape of the FMR spectra and their angular variation for the textured nanoparticle samples are strongly dependent on the particle-size and intrinsic magnetocrystalline anisotropy. In spite of this fact, in our measurements one observes that the experimental shift of the FMR line, corresponding to the change of the geometry from $H_{\parallel}$ to $H_{\perp}$ is smaller than the theoretically expected one due to the intrinsic demagnetization field. For example, Ramos *et al.*[26] reported the angular variation of the FMR spectra for continuous Ni nanowires where the magnitude of the effective anisotropy field is consistent with the structural data given by $H_A = 2M_S(1-3f)$, where f is the filling factor. This apparent reduction of local anisotropy in our samples can be explained by the fact that inside of each nanotube of AAO or BTO, the nanoparticles are not in a coalescent state, and the local anisotropy axis of these particles is randomly oriented, more likely with flocculate condition of nanoparticles. Similar results were obtained for the infiltrated samples of AAO-$MnFe_2O_4$, BTO-$MnFe_2O_4$, and PO-$MnFe_2O_4$ samples (Fig. 4). In the case of $CoFe_2O_4$ powder and infiltrated samples, the FMR signals could not be measured within the 0-2 T field range due to the very high intrinsic magnetocrystalline anisotropy field. Therefore, from the FMR spectra one clearly observes the dual nature of the infiltrated systems: (i) On one hand the cooperative or collective effect are visible through angular dependence of the FMR resonance line; (ii) On the other hand the individual particle contribution is induced by the different magnetocrystalline anisotropy for each NP systems and revealed by the weaker than expected angular variation of the resonance field for a fully oriented systems; this is, a result of the random orientation of the anisotropy axis of the nanoparticles inside of the AAO and BTO nanotubes. The interplay between both collective and individual contributions on the full magnetization is reflected in the dynamic magnetization response of these samples, which is discussed in Sec. III D.

D. Ac-susceptibility (10 Hz-10 kHz)

Magnetic susceptibility versus temperature experiments with different field amplitudes ($H = 3$, 5, and 10 Oe) and frequencies ($\nu = 10$ Hz-10 kHz) were carried out for the characterization of the dynamic response of the three batches of PO-, AAO-, and BTO-ferrite samples. Since the actual response of the sample to an applied *ac*-field is measured, the magnetodynamics can be studied through the complex susceptibility ($\chi' + j\chi''$). The real component χ' represents the component of the susceptibility that is in phase with the applied *ac*-field, while χ'' represents the component that is out of phase. The imaginary component χ'' is related to the energy loss, or in other words to the energy absorbed by the sample from the *ac* field. Figure 5 shows T-dependence of the real component of the susceptibility with an applied *ac*-field of $H_{ac} = 5$ Oe ($4\,\mathrm{K} < \mathrm{T} < 300\,\mathrm{K}$). Similar results were observed for H_{ac} strengths of 3 Oe and 10 Oe (figures not shown). Overall, the χ' vs T shows a single peak for each sample positioned at $T_{max} = T_B$. The peak shifts to higher temperatures, and its intensity diminishes as the frequency is

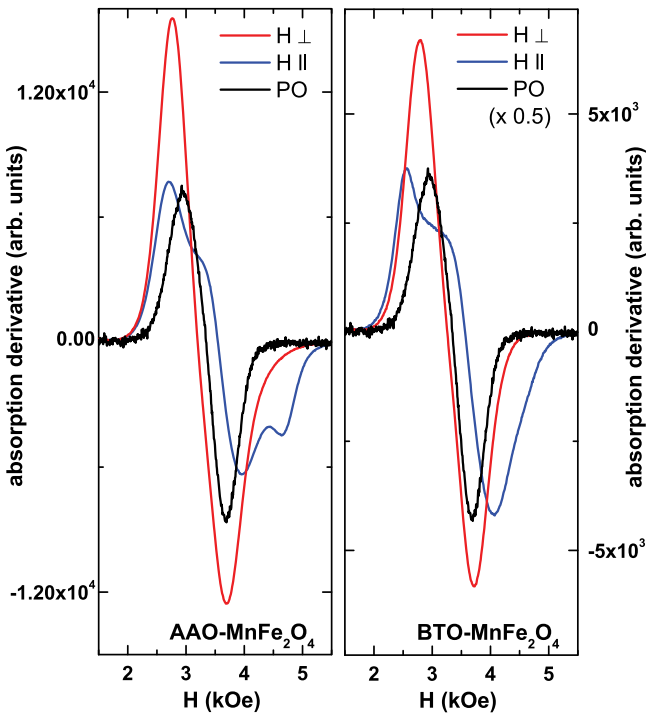

FIG. 4. X-band (9.8 GHz), FMR spectra of the $MnFe_2O_4$ NPs infiltrated into the AAO and BTO hosts. The measurements were done with magnetic field parallel ($\parallel$) and perpendicular ($\perp$) to the nanochannels. For reference control, the spectrum of the PO sample is added in both cases.

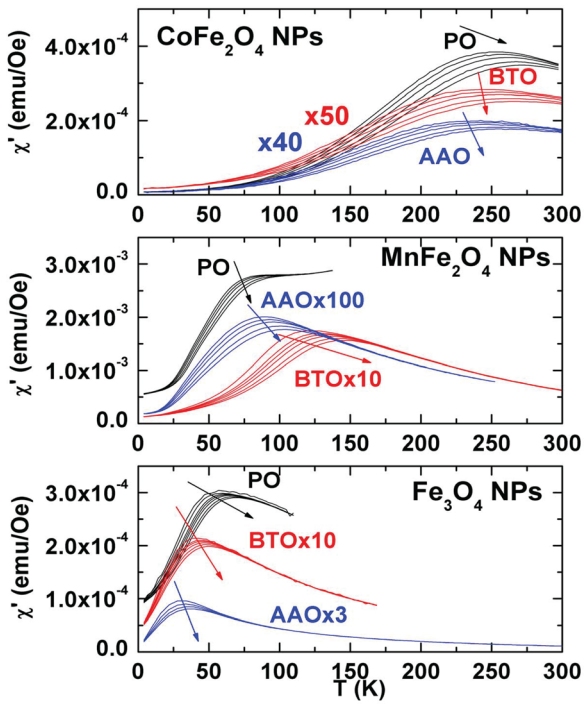

FIG. 5. T-dependence of the real part of the *AC*-susceptibility with an applied of $H_{ac} = 5$ Oe ($4\,\mathrm{K} < \mathrm{T} < 300\,\mathrm{K}$), for the three batches of ferrite samples, PO, AAO, and BTO. The arrows indicate the peak shift to higher temperatures with the increase of frequency.

increased from $\nu = 10\,\text{Hz}$ to $10\,\text{kHz}$. This effect is directly related with the frequency dependence of the blocking temperature of magnetic monodomain NPs, as the samples are cooled down.[7,8] Moreover, the rates of the peak shift with frequency are different for the three types of samples (the arrows in Fig. 5 suggest the rate of the peak-position shift as the frequency increase). In particular, comparing the χ' vs T plots for Fe_3O_4, $MnFe_2O_4$, and $CoFe_2O_4$ samples one observes that the susceptibility peaks as function of frequency are located in different temperature ranges, this being a direct correlation with the intrinsic anisotropy values.[7,8]

Two criteria have often been used for comparing the frequency dependence of T_B, namely, $C_1 = \frac{\Delta T_B}{T_B \Delta \log_{10}\nu}$, independent of any model, and $C_2 = \frac{T_B - T_0}{T_B}$, where T_0 is the characteristic temperature of the Vogel-Fulcher law described below. This law is phenomenological and without physical meaning near T_0, but C_2 can be useful for comparing the T_B trends among these samples. Figure 6 shows the variation of the T_B in the classical plot of $\text{Log}_{10}(\tau)$ vs $1/T_B$ for the three batches of samples, which in terms of the superparamagnetic Néel model (Néel 1949), the linear fit corresponds to the Arrhenius law

$$\ln\left(\frac{\tau}{\tau_0}\right) = \frac{E_B}{k_B T}, \tag{1}$$

where in a first approach τ_0 is a constant ($10^{-9}\,\text{s} < \tau_0 < 10^{-12}\,\text{s}$) and E_B is the energy barrier of the NPs. Hence, $E_B = K\bar{V}$, where K is the effective anisotropy constant. Therefore, the values of E_B and K were calculated from these experimental results. The parameters are summarized in Table II (batch of Fe_3O_4 samples), Table III (batch of $MnFe_2O_4$ samples), and Table IV (batch of $CoFe_2O_4$ samples).

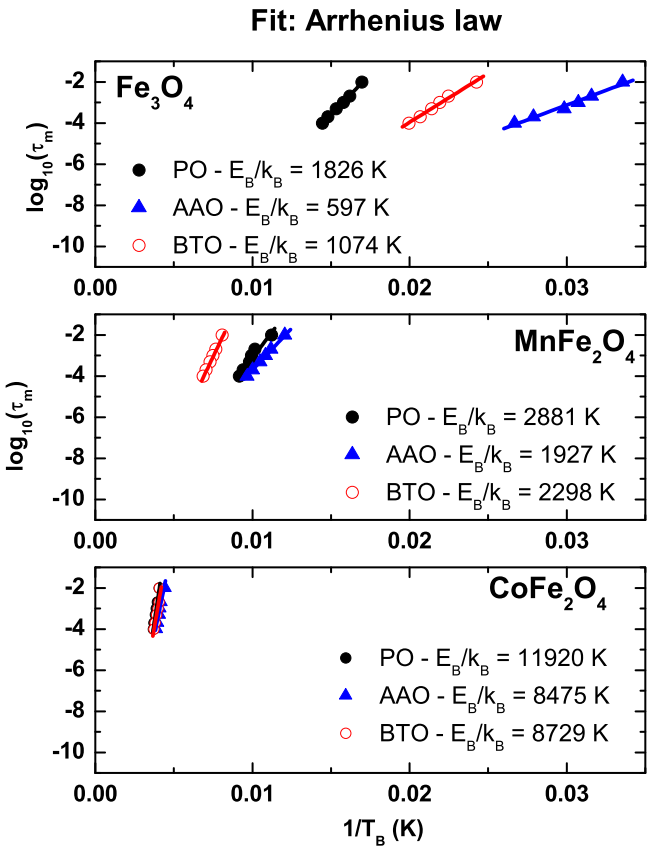

FIG. 6. The dynamic response of the magnetization, in the plot of $\log_{10}(\tau)$ against $1/T_B$, for the three batches of samples, where the linear fit corresponds to the Arrhenius law model.

TABLE II. Fe_3O_4 samples: C_1, C_2, and fit parameters coming from the Arrhenius, Fulcher, and power laws.

Sample	Arrhenius	Fulcher	Power law
PO-Fe_3O_4	$\tau_0 = 10^{-15}\,\text{s}$	$\tau_0 = 10^{-10}\,\text{s}$	$\tau_0^* = 4.1 \times 10^{-6}\,\text{s}$
	$E_B = 1825.7\,\text{K}$	$E_B = 602.2\,\text{K}$	$z\nu = 10.7$
	...	$T_0 = 26.2\,\text{K}$	$T_g = 39.4\,\text{K}$
	$C_1 = 0.08$	$C_2 = 0.61$	...
BTO-Fe_3O_4	$\tau_0 = 10^{-13}\,\text{s}$	$\tau_0 = 10^{-10}\,\text{s}$	$\tau_0^* = 4.8 \times 10^{-7}\,\text{s}$
	$E_B = 1073.7\,\text{K}$	$E_B = 443.5\,\text{K}$	$z\nu = 7.4$
	...	$T_0 = 18.0\,\text{K}$	$T_g = 33.6\,\text{K}$
	$C_1 = 0.10$	$C_2 = 0.63$	...
AAO-Fe_3O_4	$\tau_0 = 10^{-11}\,\text{s}$	$\tau_0 = 10^{-10}\,\text{s}$	$\tau_0^* = 3.4 \times 10^{-6}\,\text{s}$
	$E_B = 597.3\,\text{K}$	$E_B = 497.7\,\text{K}$	$z\nu = 4.1$
	...	$T_0 = 2.1\,\text{K}$	$T_g = 26.1\,\text{K}$
	$C_1 = 0.16$	$C_2 = 0.94$	...

Although the fitted straight-lines in Fig. 6 seem to be in good agreement with the experimental data, the Arrhenius law output fit parameters have no physical significance. Specifically, the τ_0 values are much smaller than the physically accepted ones and E_B values are relatively high compared with the reference values[27,28] of $E_B = 303\,\text{K}$ (Fe_3O_4, using $K = 2.43 \times 10^5\,\text{erg/cm}^3$), $E_B = 280\,\text{K}$ ($MnFe_2O_4$, using $K = 8.5 \times 10^4\,\text{erg/cm}^3$), and $E_B = 3885\,\text{K}$ ($CoFe_2O_4$, using $K = 2.0 \times 10^6\,\text{erg/cm}^3$). Consequently the experimentally observed variation of *ac* susceptibility for all samples is not consistent with a simple superparamagnetic blocking behavior of independent particles.

Dormann and Fiorani proved that in the case of cluster-like particles the interaction effect cannot be neglected, where different scaling laws based in phenomenological models and Néel theory for intermediate and strong interacting systems were tested.[12,13] Following the same work of Dormann and co-workers in order to treat the interaction and collective effects, in this paper we analyze the *ac*

TABLE III. $MnFe_2O_4$ samples: C_1, C_2, and fit parameters coming from the Arrhenius, Fulcher, and power laws.

Sample	Arrhenius	Fulcher	Power law
PO-$MnFe_2O_4$	$\tau_0 = 10^{-15}\,\text{s}$	$\tau_0 = 10^{-10}\,\text{s}$	$\tau_0^* = 10^{-6}\,\text{s}$
	$E_B = 2881.0\,\text{K}$	$E_B = 657.8\,\text{K}$	$z\nu = 2.6$
	...	$T_0 = 59.3\,\text{K}$	$T_g = 93.2\,\text{K}$
	$C_1 = 0.08$	$C_2 = 0.44$	...
BTO-$MnFe_2O_4$	$\tau_0 = 10^{-13}\,\text{s}$	$\tau_0 = 10^{-10}\,\text{s}$	$\tau_0^* = 8.1 \times 10^{-7}\,\text{s}$
	$E_B = 2298.2\,\text{K}$	$E_B = 1245.1\,\text{K}$	$z\nu = 8.6$
	...	$T_0 = 56.2\,\text{K}$	$T_g = 92.8\,\text{K}$
	$C_1 = 0.09$	$C_2 = 0.60$	...
AAO-$MnFe_2O_4$	$\tau_0 = 10^{-12}\,\text{s}$	$\tau_0 = 10^{-10}\,\text{s}$	$\tau_0^* = 1.0\,\text{s}$
	$E_B = 1927.0\,\text{K}$	$E_B = 1101.0\,\text{K}$	$z\nu = 12.4$
	...	$T_0 = 24.0\,\text{K}$	$T_g = 37.2\,\text{K}$
	$C_1 = 0.11$	$C_2 = 0.76$	...

TABLE IV. $CoFe_2O_4$ samples: C_1, C_2, and fit parameters coming from Arrhenius, Fulcher, and power laws.

Sample	Arrhenius	Fulcher	Power law
PO-$CoFe_2O_4$	$\tau_0 = 10^{-23}$ s	$\tau_0 = 10^{-10}$ s	$\tau_0^* = 2.7 \times 10^{-9}$ s
	$E_B = 11919.6$ K	$E_B = 1589.0$ K	$z\nu = 11.2$
	...	$T_0 = 158.7$ K	$T_g = 195.4$ K
	$C_1 = 0.05$	$C_2 = 0.41$	...
BTO-$CoFe_2O_4$	$\tau_0 = 10^{-18}$ s	$\tau_0 = 10^{-10}$ s	$\tau_0^* = 1.0$ s
	$E_B = 8728.5$ K	$E_B = 1218.0$ K	$z\nu = 20.2$
	...	$T_0 = 133.6$ K	$T_g = 104.1$ K
	$C_1 = 0.07$	$C_2 = 0.49$	...
AAO-$CoFe_2O_4$	$\tau_0 = 10^{-18}$ s	$\tau_0 = 10^{-10}$ s	$\tau_0^* = 2.5 \times 10^{-8}$ s
	$E_B = 8475.2$ K	$E_B = 1381.9$ K	$z\nu = 4.8$
	...	$T_0 = 156.6$ K	$T_g = 217.6$ K
	$C_1 = 0.07$	$C_2 = 0.38$	...

susceptibility data using the Vogel-Fulcher and power laws coming from the spin-glass literature.[12,13]

The observed slowing down of relaxation process in our samples can be addressed by the Vogel-Fulcher law describing a divergence of the relaxation time at finite temperature T_0. The Vogel-Fulcher law is given by

$$\tau = \tau_0 \exp\left(\frac{E_B}{k_B(T - T_0)}\right), \quad (2)$$

and it is valid only if $T \gg T_0$, where T_0 is a temperature proportional to the power of the internal molecular field and increases with the interaction strength. Hence, for $T_0 = 0$, it gives the Arrhenius law. Taking into account Eq. (2), the obtained fitted parameters are summarized in Table II (batch of Fe_3O_4 samples), Table III (batch of $MnFe_2O_4$ samples), and Table IV (batch of $CoFe_2O_4$ samples) and can be compared with the parameters coming from the Arrhenius law discussed above. Also, the parameters C_1 and C_2 are indicated in each table, respectively. Figure 7 shows the adjusted curves for the three batches of samples, following the Vogel-Fulcher law.

The Vogel-Fulcher law provides more reasonable values for τ_0 and T_0, as those observed in spin glasses. Analyzing the variation of C_1 and C_2 coefficients across all the samples one observes a systematic increase in their values as the nanoparticles are infiltrated into the BTO and AAO templates which is consistent with a decrease of the interactions in these samples. Powder samples give the smallest coefficients due to the three dimensional interaction between the particles. The intermediate values for C_1 and C_2 in the case of BTO and AAO infiltrated samples are comparable with those reported by Dormann and Fiorani,[7,8] for flocculated-like nanoparticles. In particular, values of the C_2 parameter between 0.3 and 0.6 were observed for inhomogeneous freezing similarly with the infiltrated samples due to geometrical confinement. In fact Saslow[29] presented a scenario to theoretically explain the Vogel-Fulcher law by using a Landau free energy together with a linear coupling to a random field, which can be correlated with the randomness of inhomogeneous freezing processes.

The values of C_1 and C_2 suggest that our magnetic nanoparticle systems are subject to magnetic interactions of different strengths which for some of the samples may be large enough to promote a super-spin glass transition, as observed by Parker *et al.*[15] In order to check this hypothesis we fit the *ac* susceptibility data with the power law $\tau = \tau_0^* \left(\frac{T_g}{T_{max} - T_g}\right)^{z\nu}$ describing a second order phase transition with a divergence of a correlation length. The results of the fit are displayed in Figure 8 with the fit parameters summarized in Tables II (Fe_3O_4 samples), Table III ($MnFe_2O_4$ samples), and Table IV ($CoFe_2O_4$ samples).

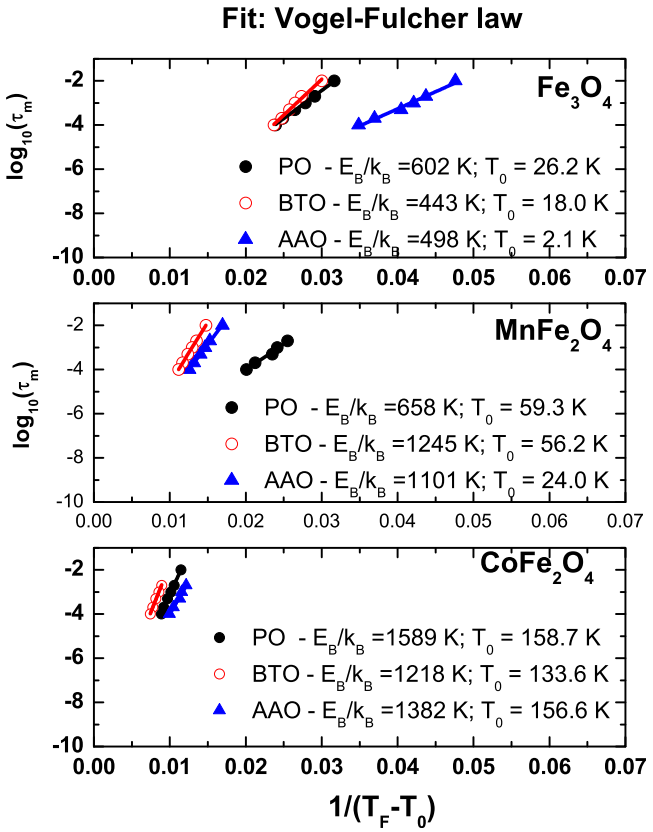

FIG. 7. The dynamic response of the magnetization, in the plot of $\log_{10}(\tau)$ against $1/(T_B - T_0)$, for the three batches of samples, where the linear fit corresponds to the Fulcher law model.

From the obtained power law fit parameters one observes a different behavior for each of magnetic nanoparticles systems. In the case of Fe_3O_4 nanoparticle samples, all three systems, powder, BTO and AAO provide reasonable values for the critical exponent $z\nu$ and prefactor τ_0^*. The critical exponent $z\nu$ values range from 10.7 to 4.1 with a scaling according to the different strength of interactions in the three samples. Thus, the largest value of $z\nu$ is obtained for PO-Fe_3O_4 sample which is expected to have the strongest interactions between nanoparticles whilst the smaller values is obtained in the case of AAO-Fe_3O_4 sample where the nanoparticles are confined in nanochannels with the largest diameter. The large value of τ_0^* can be explained by considering it to be temperature dependent following an Arrhenius type law,[30,31] i.e., $\tau_0^*(T) \sim \tau_0 \exp(E_B/k_BT)$. Considering $\tau_0 = 10^{-9}$ s at $T_g = 40.0$ K and for $E_B = 300$ K one obtains $\tau_0^*(T_g) \approx 10^{-6}$ s. For $MnFe_2O_4$ and $CoFe_2O_4$ samples, only for the BTO-$MnFe_2O_4$, PO-$CoFe_2O_4$, and AAO-$CoFe_2O_4$, one obtained fit parameters plausible for a spin glass system, supporting the existence of phase transition from a superparamagnetic state to a SSG state and close to

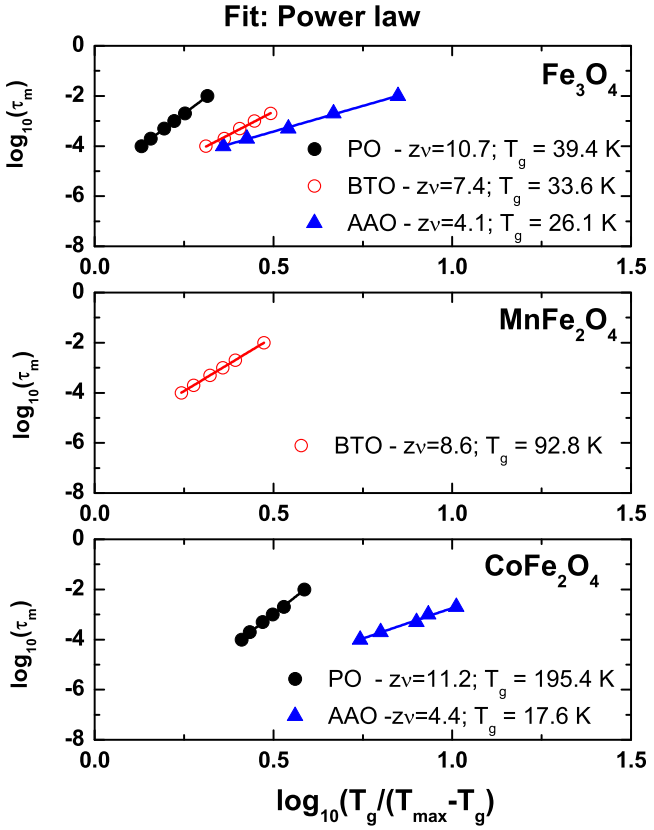

FIG. 8. The dynamic response of the magnetization, in the plot of $\log_{10}(\tau)$ against $\log_{10}(T_g/(T_{max}-T_g))$, for the three batches of samples, where the linear fit corresponds to the power law model.

values already reported in the case of other SSGs.[32,33] Critical slowing down, as expressed by the power law, cannot explain the *ac* susceptibility data for all magnetic nanoparticle systems due to the different competition between the intrinsic and collective properties in the studied samples.

IV. CONCLUSIONS

We have shown, by using dynamic magnetization techniques as *ac* susceptibility and FMR in addition to *dc*-magnetization curves, that it is conceivable to tune the collective behavior of the confined NPs by a control of the intrinsic properties of NPs and their spatial arrangement. The confinement effects were studied by considering three different geometries of nanoparticles. Specifically, we considered Fe_3O_4, $MnFe_2O_4$, and $CoFe_2O_4$ single magnetic domain NPs with size near to 10 nm, infiltrated into AAO templates with 297 nm porous size and thickness of 50 μm, and infiltrated in an non-magnetic AAO-BTO nanotubes with 197 nm internal porous size and same length. FMR experiments on the infiltrated AAO templates and BTO nanotubes yields direct information about the interplay between the individual and cooperative or collective contributions, which can be related to the array structure and texturization. The experimentally observed variation of *ac* susceptibility for all samples is not consistent with a simple superparamagnetic blocking behavior of independent particles following the Arrhenius law. The observed slowing down of the relaxation process in our samples suggests that a SSG can be induced by increased magnetic interactions through a competition between intrinsic properties of nanoparticles and their reciprocal spatial arrangement.

ACKNOWLEDGMENTS

This work was supported by the National Science Foundation, through the LASiGMA project grants (No. EPS 1003897) and Louisiana Board of Regents Contract No. LEQSF(2007-12)-ENH-PKSFI-PRS-04.

[1]D. Fiorani, J. L. Dormann, R. Cherkaoui, E. Tronc, F. Lucari, F. D'Orazio, L. Spinu, M. Nogues, A. Garcia, and A. M. Testa, J. Magn. Magn. Mater. **196**, 143 (1999).
[2]J. L. Dormann, D. Fiorani, R. Cherkaoui, E. Tronc, F. Lucari, F. D'Orazio, L. Spinu, M. Nogues, H. Kachkachi, and J. P. Jolivet, J. Magn. Magn. Mater. **203**, 23 (1999).
[3]R. P. Cowburn and M. E. Welland, Science **287**, 1466 (2000).
[4]V. Castel, C. Brosseau, and J. B. Youssef, J. Appl. Phys. **106**, 064312 (2009).
[5]R. P. Cowburn, Phys. Rev. B **65**, 092409 (2002).
[6]T. Jonsson, P. Svedlindh, and M. F. Hansen, Phys. Rev. Lett. **81**, 3976 (1998).
[7]J. L. Dormann, L. Bessaist, and D. Fiorani, J. Phys. C: Solid State Phys. **21**, 2015 (1988).
[8]J. L. Dormann, D. Fiorani, and E. Tronc, J. Magn. Magn. Mater. **202**, 251 (1999).
[9]A. Encinas-Oropesa, M. Demand, L. Piraux, I. Huynen, and U. Ebels, Phys. Rev. B **63**, 104415 (2001).
[10]J. Escrig, J. Bachmann, J. Jing, M. Daub, D. Altbir, and K. Nielsch, Phys. Rev. B **77**, 214421 (2008).
[11]R. F. Neumann, M. Bahiana, J. Escrig, S. Allende, K. Nielsch, and D. Altbir, Appl. Phys. Lett. **98**, 022502 (2011).
[12]D. Fiorani, J. Tholence, and J. L. Dormann, J. Phys. C **19**, 5495 (1986).
[13]D. Fiorani, J. L. Dormann, J. L. Tholence, L. Bessais, and D. Villers, J. Magn. Magn. Mater. **54**, 173 (1986).
[14]S. Mørup, Europhys. Lett. **28**, 671 (1994).
[15]D. Parker, V. Dupuis, F. Ladieu, J.-P. Bouchaud, E. Dubois, R. Perzynski, and E. Vincent, Phys. Rev. B **77**, 104428 (2008).
[16]V. Skumryev, S. Stoyanov, Y. Zhang, G. Hadjipanayis, D. Givord, and J. Nogués, Nature (London) **423**, 850 (2003).
[17]J. Sort, V. Langlais, S. Doppiu, B. Dieny, S. Suriñach, J. S. Muñoz, M. D. Baró, C. H. Laurent, and J. Nogués, Nanotechnology **15**, S211 (2004).
[18]J. M. Vargas, J. Gómez, R. D. Zysler, and A. Butera, Nanotechnology **18**, 115714 (2007).
[19]M. Pasquale, E. S. Olivetti, M. Coisson, P. Rizzi, and G. Bertotti, J. Appl. Phys. **103**, 07D527 (2008).
[20]A. F. Gross, M. R. Diehl, K. C. Beverly, E. K. Richman, and S. H. Tolbert, J. Phys. Chem. B **107**, 5475 (2003).
[21]J.-S. Jung, J.-H. Lim, L. Malkinski, A. Vovk, K.-H. Choi, S.-L. Oh, Y.-R. Kim, and J.-H. Jund, J. Magn. Magn. Mater. **310**, 2361 (2007).
[22]A. Yourdkhani and G. Caruntu, J. Mater. Chem. **21**, 7145 (2011).
[23]J. M. Vargas, A. Srivastava, A. Yourdkhani, L. Zaldivar, G. Caruntu, and L. Spinu, J. Appl. Phys. **110**, 064304 (2011).
[24]H. Lu, W. T. Zheng, and Q. Jiang, J. Phys. D: Appl. Phys. **40**, 320 (2007).
[25]J. M. Vargas, E. Lima, Jr., R. D. Zysler, J. G. S. Duque, E. De Biasi, and M. Knobel, Eur. Phys. J. B **64**, 211 (2008).
[26]C. A. Ramos, M. Vazquez, K. Nielsch, K. Pirota, J. Rivas, R. B. Wehrspohn, M. Tovar, R. D. Sanchez, and U. Gøsele, J. Magn. Magn. Mater. **272**, 1652 (2004).
[27]S. Yoon and K. M. Krishnan, J. Appl. Phys. **109**, 07B534 (2011).
[28]E. Lima, Jr., A. L. Brandl, A. D. Arelaro, and G. F. Goya, J. Appl. Phys. **99**, 083908 (2006).
[29]W. M. Saslow, Phys. Rev. B **37**, 676 (1988).
[30]S. Nakamae, Y. Tahri, C. Thibierge, D. L'Hote, E. Vincent, V. Dupuis, E. Dubois, and R. Perzynski, J. Appl. Phys. **105**, 07E318 (2009).
[31]P.-M. Dejardin, J. Appl. Phys. **110**, 113921 (2011).
[32]P. Jonsson, M. F. Hansen, P. Svedlindh, and P. Nordblad, J. Magn. Magn. Mater. **226**, 1315 (2001).
[33]K. Hiroi, K. Komatsu, and T. Sato, Phys. Rev. B **83**, 224423 (2011).